Supplementary Text: Identifiability of Differential-Algebraic Systems

Arthur N. Montanari [a], François Lamoline [b], Robert Bereza [c], Jorge Gonçalves [b,d]

[a] *Department of Physics and Astronomy, Northwestern University, Evanston, IL 60208, USA*

[b] *Luxembourg Centre for Systems Biomedicine, University of Luxembourg, Belvaux L-4367, Luxembourg*

[c] *Division of Decision and Control Systems, KTH Royal Institute of Technology, Stockholm SE-100 44, Sweden*

[d] *Department of Plant Sciences, Cambridge University, Cambridge CB2 3EA, United Kingdom*

S1 Identifiability analysis of chemical reactor

Consider an exothermic reactor system with a single first-order reaction (A $\xrightarrow{r(t)}$ B) and generated heat removed through an external cooling circuit. The chemical reactor is modeled by [1]

$$\dot{x}_1 = k_1(c_0 - x_1) - x_3 \tag{S1a}$$
$$\dot{x}_2 = k_1(T_0 - x_2) + k_2 x_3 + k_3(T_c - x_2), \tag{S1b}$$
$$0 = x_3 - k_5 \exp\{-k_4/x_2\} x_1, \tag{S1c}$$

where $\boldsymbol{x} = [x_1 \ x_2 \ x_3]^\mathsf{T} \in \mathbb{R}^3$ is the state vector, x_1 is the concentration of reactant A, x_2 is the temperature, and x_3 is the reaction rate per unit volume (algebraic variable). Eq. (S1c) arises from a conservation law [1] (Arrhenius equation) that imposes the dependence of reaction rates on temperature. The parameters are: inlet feed reactant concentration c_0 and feed temperature T_0, coolant temperature T_c, and other constants k_i. Fig. S2 shows that the chemical reactor dynamics converge to a limit cycle for the considered set of parameters.

Let the coolant temperature be the parameter sought to be identified (i.e., $\theta = T_c$). The accuracy of parameter estimation depends on the choice of observable, that is, which state variable x_i is measured by a sensor. To determine the most suitable sensor data for parameter estimation, we now test which observables ensure parameter identifiability. As a tutorial, we analyze the identifiability of the descriptor model (S1) step-by-step, considering the output signal $y(t) = x_1(t)$, $t \in [0, 10]$ s. First, we augment model (S1) by representing $\theta(t) = T_c(t)$ as an additional state variable with constant dynamics, i.e., $\dot{\theta}(t) = 0$. Functions $\bar{\boldsymbol{H}}_\nu$ and $\bar{\boldsymbol{F}}_\mu$ are then constructed up to order $\mu = \nu = n + p - 1 = 3$. Thus, $\bar{\boldsymbol{H}}_\nu = [x_1 \ \dot{x}_1 \ \ddot{x}_1]^\mathsf{T}$ and $\bar{\boldsymbol{F}}_\mu = [(\boldsymbol{F})^\mathsf{T} \ (\frac{\mathrm{d}\boldsymbol{F}}{\mathrm{d}t})^\mathsf{T} \ (\frac{\mathrm{d}^2\boldsymbol{F}}{\mathrm{d}t^2})^\mathsf{T}]^\mathsf{T}$, where

[1] This descriptor model can be directly converted to ODEs and then numerically integrated with conventional solvers (e.g., 4th-order Runge-Kutta). However, numerical solvers for DAEs enforce the constraint (S1c) to be preserved in simulations as in Fig. S2.

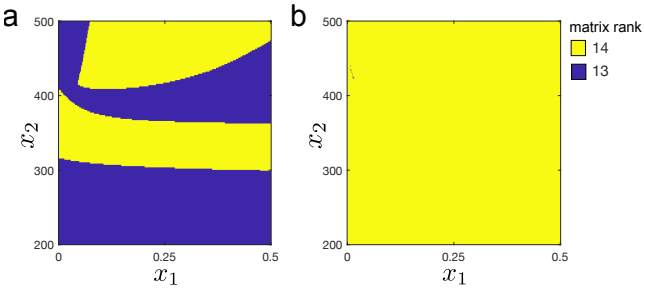

Fig. S1. Numerical values corresponding to **(a)** the left-hand side (LHS) and **(b)** the right-hand side (RHS) of Eq. (12) locally evaluated at each state $\boldsymbol{x}$ in the phase plane (x_1, x_2). The tolerance for the numerical rank computation is set to $\max_{\boldsymbol{x}} \sigma n\epsilon(\|\mathcal{I}(\theta, \boldsymbol{z})\|_2) = 10^{-6}$, where $\epsilon(\cdot)$ indicates the floating-point relative accuracy of a number. This tolerance ensures that the rank analysis is consistent for all states $(x_1, x_2) \in [0,\ 0.5] \times [200,\ 500]$.

$$\boldsymbol{F} = \begin{bmatrix} k_1(c_0 - x_1) - x_3 - \dot{x}_1 \\ k_1(T_0 - x_2) + k_2 x_3 + k_3(\theta - x_2) - \dot{x}_2 \\ x_3 - k_5 \exp\left\{-\frac{k_4}{x_2}\right\} x_1 \\ \dot{\theta} \end{bmatrix},$$

$$\frac{\mathrm{d}\boldsymbol{F}}{\mathrm{d}t} = \begin{bmatrix} -k_1\dot{x}_1 - \dot{x}_3 - \ddot{x}_1 \\ -k_1\dot{x}_2 + k_2\dot{x}_3 + k_3(\dot{\theta} - \dot{x}_2) - \ddot{x}_2 \\ \dot{x}_3 - k_5 \exp\left\{-\frac{k_4}{x_2}\right\} \left(\dot{x}_1 + k_4 \frac{x_1 \dot{x}_2}{x_2^2}\right) \\ 0 \end{bmatrix},$$

and $\mathrm{d}^i\boldsymbol{F}/\mathrm{d}t^i$, $i \geq 2$, is omitted for the sake of brevity. Note that $\bar{\boldsymbol{F}}_\mu$ and $\bar{\boldsymbol{H}}_\nu$ are functions of θ, $\boldsymbol{x}$, and its time derivatives. By assumption, $\dot{\theta} = \ddot{\theta} = \dddot{\theta} = 0$, $\forall t$. After building the identifiability matrix (11), condition (12) can then be locally evaluated to test if the system is identifiable at any consistent state $\boldsymbol{x}_0 \in \mathbb{L} \subset \mathbb{R}^3$ and parameter value $\theta_0 \in \mathbb{R}^1$. Fig. S1a shows the rank of the iden-

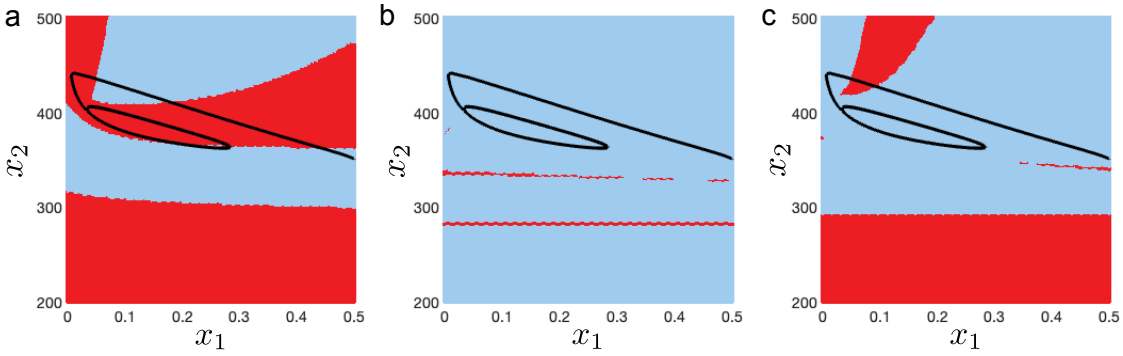

Fig. S2. Identifiable regions of the chemical reactor model for measurement signals given by: **(a)** $y = x_1$, **(b)** $y = x_2$, and **(c)** $y = x_3$. The blue (red) colors correspond to states $\boldsymbol{x}$ in which the parameter T_c is identifiable (unidentifiable). The black solid line represents the state trajectory $\boldsymbol{x}(t)$ starting at the initial condition $\boldsymbol{x}(0) = [0.5\ 350\ 0.4995]^\mathsf{T}$ and converging to a limit cycle. The system parameters were set to $(c_0, T_0, T_c) = (1, 350, 305)$, and $(k_1, k_2, k_3, k_4, k_5) = (1, 209.205, 2.0921, 8.7503{\cdot}10^3, 7.2{\cdot}10^{10})$. The numerical simulations are shown using the `ode15s` solver in MATLAB.

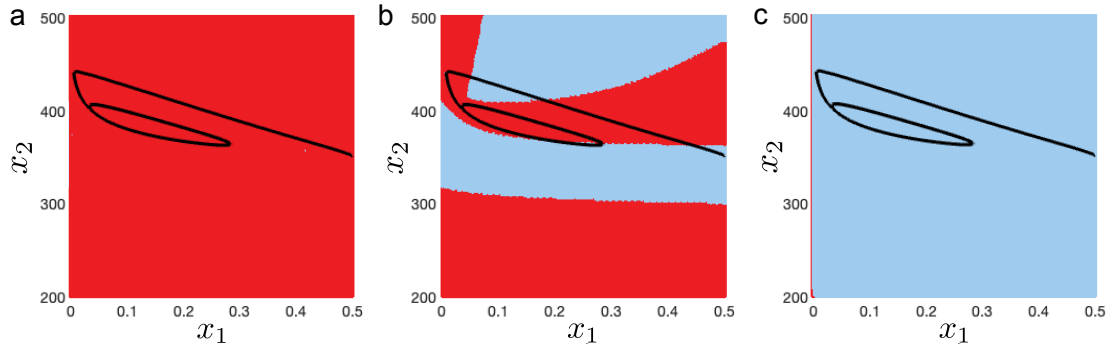

Fig. S3. Identifiable regions of the chemical reactor for different choices of rank tolerances: **(a)** 10^{-1}, **(b)** 10^{-6}, **(c)** 10^{-15}. The blue (red) colors correspond to states $\boldsymbol{x}$ in which the parameter T_c is identifiable (unidentifiable) using sensor $y = x_1$.

tifiability matrix $\mathcal{I}(\boldsymbol{\theta}, \boldsymbol{z})$ for every state $\boldsymbol{x}$ in the phase plane (x_1, x_2). The local identifiability of $\boldsymbol{\theta}$ is guaranteed for states in which the computed LHS (Fig. S1a) and RHS (Fig. S1b) of Eq. (12) are equal.

Fig. S2 shows the identifiable and unidentifiable regions in the state space depending on the observable choice. For the output $y(t) = x_1(t)$ (Fig. S2a), the limit cycle solution $\boldsymbol{\Phi}(\boldsymbol{x}(0); \theta)$ lies predominantly in an unidentifiable region. Following Definition 4, at an unidentifiable state $\boldsymbol{x}_0$, measured trajectories $\boldsymbol{h} \circ \boldsymbol{\Phi}(\boldsymbol{x}_0; \theta)$ sufficiently close to $\boldsymbol{x}_0$ are *not* guaranteed to be distinguishable from a trajectory $\boldsymbol{h} \circ \boldsymbol{\Phi}(\boldsymbol{x}_0; \theta')$ corresponding to some distinct parameter $\theta' \neq \theta$ lying in a neighborhood $\mathcal{U}$ of the true parameter value θ. In other words, there may exist some $(\theta' \in \mathcal{U}) \neq \theta$ such that $\boldsymbol{h} \circ \boldsymbol{\Phi}(\boldsymbol{x}_0; \theta) = \boldsymbol{h} \circ \boldsymbol{\Phi}(\boldsymbol{x}_0; \theta')$. The predominance of unidentifiable regions in the state space implies the possible existence of non-unique solutions for θ in the neighborhood of $\boldsymbol{\Phi}(\boldsymbol{x}(0); \boldsymbol{\theta})$. As a result, if the dataset primarily comprises measurement data collected from these unidentifiable states, the estimation accuracy of θ may be compromised.

Despite the predominance of unidentifiable regions in Fig. S2a, parameter identifiability is achieved in a small region of the limit cycle around $\boldsymbol{x} = [0.25\ 360\ 0.5]^\mathsf{T}$ (as well as other regions containing part of the transient response). Theoretically, parameter estimation could be possible by using data collected solely at these identifiable states. However, this may not be possible in practice if the identifiable region is too small (as in Fig. S2a) due to limited data availability. Moreover, we note that such analysis depends on the choice of tolerances for the rank computation, as presented in Fig. S1. Regions of identifiable/unidentifiable states may expand or shrink depending on the tolerance value. This dependence is illustrated in Fig. S3. If the rank tolerances are not appropriately chosen, condition (12) may be numerically satisfied for ill-conditioned matrices $\mathcal{I}(\boldsymbol{\theta}, \boldsymbol{z})$, even when the system is practically unidentifiable.

After conducting the same identifiability analysis for $y(t) = x_2(t)$ and $y(t) = x_3(t)$, Fig. S2b,c shows that the system is locally identifiable everywhere around the limit cycle solution when these other types of measurement signals (sensors) are considered. This is a particularly beneficial result for this sensor placement problem, since temperature sensors $(y = x_2)$ are very affordable and practical to install in chemical reactors.

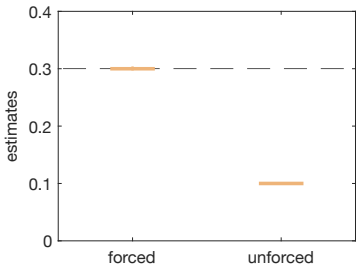

Fig. S4. Parameter estimation of mass m using the prediction-error method for DAE system identification. The estimates are shown for data collected from the angle trajectories of forced and unforced pendulums. The estimate is computed for 100 independent datasets, each with 500 data samples.

S2 Parameter estimation of a pendulum

We describe the numerical setup employed to generate the data used for the pendulum's parameter estimation.

Data generation. The data used for the parameter estimation experiment in Fig. 3 is generated using the pendulum model with an external force applied in the x-direction. The complete equations of the forced pendulum are given by

$$\dot{x}_1 = x_3, \tag{S2a}$$
$$\dot{x}_2 = x_4, \tag{S2b}$$
$$\dot{x}_3 = \frac{x_1 x_5}{m} + \frac{u}{m}, \tag{S2c}$$
$$\dot{x}_4 = \frac{x_2 x_5}{m} - g, \tag{S2d}$$
$$0 = x_1^2 + x_2^2 - L^2, \tag{S2e}$$

where u is the time-varying input force affecting the pendulum. In addition, the measurement samples are disturbed by i.i.d. samples of zero-mean Gaussian noise with variance 0.002, denoted by $v(t_k)$, so that

$$y(t_k) = \arctan\left(-\frac{x_1(t_k)}{x_2(t_k)}\right) + v(t_k).$$

By using independent realizations of the measurement noise v, 100 independent datasets are generated for the experiment. The initial conditions of the simulation are $\boldsymbol{x}(0) = [0 \ -L \ 0 \ 0 \ 0]^\top$, and the input $u(t)$ is generated exactly as reported in Ref. [2].

Parameter estimation. To numerically estimate the parameters from data, the mean square error between a measured noisy trajectory and a trajectory predicted by the model is minimized over the model parameters in each experiment. The minimization is performed using the Levenberg-Marquardt algorithm, using the same settings as in Ref. [2]. The initial estimates for the parameters are set to $m' = 0.1$, $g' = 8.21$, and $L' = 5.41$. The prediction-error model uses the same input as the one used in the data generation (i.e., Eqs. (S2)), but no measurement noise is applied to the model output.

Identification analysis of an unforced pendulum. The parameter estimation in Fig. 3 utilizes data collected from a pendulum trajectory excited by an external drive. We show that the parameter $\theta = m$ can be successfully identified (as predicted by our theory) if enough data points are provided. We now show in Fig. S4 that identification of m is impossible if the pendulum is unforced (i.e., $u = 0$). In this scenario, the returned estimate is always 0.1. This occurs because the gradient of the cost function with respect to m evaluates to 0 in the unforced case. Consequently, the Levenberg-Marquardt algorithm converges immediately, returning the initial value $m' = 0.1$.

This result is theoretically expected. The steady-state dynamics of an unforced pendulum, assuming it was released with zero velocity ($x_3(0) = x_4(0) = 0$) and low angle ($y(0) = \tan^{-1}(-\frac{x_1(0)}{x_2(0)}) \ll 1$), are described by a simple harmonic motion. Thus, the measured angle follows the trajectory

$$y(t) = y(0)\cos\left(\sqrt{\frac{g}{L}}t\right), \tag{S3}$$

that is, a limit cycle of period $T = 2\pi\sqrt{L/g}$. Clearly, neither the measured trajectory $y(t)$ nor the period T depend on the mass m; therefore, this parameter becomes unidentifiable in such scenarios. The presence of an external drive is thus essential to sufficiently "excite" the transient dynamics of the pendulum, enabling the successful identification of m as predicted by our theory. This excitation also allows us to identify the parameters g and L separately as well, instead of only being able to identify their ratio g/L as in the unforced case.

References

[1] W. H. Ray, Advanced Process Control, New York: McGraw-Hill, 1981.

[2] R. Bereza, O. Eriksson, M. R.-H. Abdalmoaty, D. Broman, H. Hjalmarsson, Stochastic approximation for identification of non-linear differential-algebraic equations with process disturbances, IEEE Conference on Decision and Control (2022) 6712–6717.